

Novel constraints on light elementary particles and extra-dimensional physics from the Casimir effect

R. S. Decca¹, D. López², E. Fischbach³, G. L. Klimchitskaya^{4,a}, D. E. Krause^{5,3}, and V. M. Mostepanenko^{4,b}

¹ Department of Physics, Indiana University-Purdue University Indianapolis, Indianapolis, Indiana 46202, USA

² Bell Laboratories, Lucent Technologies, Murray Hill, New Jersey 07974, USA

³ Department of Physics, Purdue University, West Lafayette, Indiana 47907, USA

⁴ Center of Theoretical Studies and Institute for Theoretical Physics, Leipzig University, Augustusplatz 10/11, 04109, Leipzig, Germany

⁵ Physics Department, Wabash College, Crawfordsville, Indiana 47933, USA

Received: date / Revised version: date

Abstract. We present supplementary information on the recent indirect measurement of the Casimir pressure between two parallel plates using a micromachined oscillator. The equivalent pressure between the plates is obtained by means of the proximity force approximation after measuring the force gradient between a gold coated sphere and a gold coated plate. The data are compared with a new theoretical approach to the thermal Casimir force based on the use of the Lifshitz formula, combined with a generalized plasma-like dielectric permittivity which takes into account interband transitions of core electrons. The theoretical Casimir pressures calculated using the new approach are compared with those computed in the framework of the previously used impedance approach and also with the Drude model approach. The latter is shown to be excluded by the data at a 99.9% confidence level within a wide separation range from 210 to 620 nm. The level of agreement between the data and theoretical approaches based on the generalized plasma model, or the Leontovich surface impedance, is used to set stronger constraints on the Yukawa forces predicted from the exchange of light elementary particles and/or extra-dimensional physics. The resulting constraints are the strongest in the interaction region from 20 to 86 nm with a largest improvement by a factor of 4.4 at 26 nm.

1 Introduction

It is well known that there is little or no experimental confirmation for many predictions of unified field theories, supersymmetry, supergravity, or string theory. Direct experimental tests for many of these predictions require accelerators of very high energies which will be not available in the foreseeable future. For this reason any non-accelerator tests of the predictions of new physics beyond the standard model attract the serious attention of both experimentalists and theorists.

One of the most intriguing predictions made by many extensions of the standard model is the existence of light and massless elementary particles which arise as a result of some spontaneously (or weakly dynamically) broken symmetry. Beams of such particles can penetrate through thick matter with practically no interaction. This makes it difficult to investigate these particles using the usual laboratory setups of elementary particle physics. There is,

however, an alternative way to investigate light elementary particles and their interactions by using table-top laboratory experiments. These experiments utilize the fact that the exchange of such particles between atoms belonging to two different macrobodies can generate a new long-range force in addition to the commonly known electromagnetic and gravitational interactions. For example, the exchange of predicted light bosons, such as scalar axions, graviphotons, hyperphotons, dilatons and moduli among others (see, e.g. [1, 2, 3, 4, 5]) generates a Yukawa potential. The simultaneous exchange of two photons, two massless scalars or massless pseudoscalars, and the exchange of a massless axion or a massless neutrino-antineutrino pair leads to power-law interactions with different powers [6, 7, 8, 9, 10, 11]. Coincidentally, a Yukawa correction to Newtonian gravity is predicted in extra-dimensional physics with compact extra dimensions and low energy compactification scale of order of 1 TeV [12, 13, 14, 15]. Furthermore, some brane theories contain exactly the standard model at low energy [16]. For models of non-compact but warped extra dimensions, power-law corrections to the Newtonian gravitational law have been predicted [17]. The cosmological constant generated in such models may be of the correct order of magnitude as suggested by observations [18].

^a On leave from North-West Technical University, Millionnaya St. 5, St.Petersburg, 191065, Russia

^b On leave from Noncommercial Partnership “Scientific Instruments”, Tverskaya St. 11, Moscow, 103905, Russia

Direct experimental signatures of strings and branes are discussed in [19].

Experimental constraints on hypothetical long-range interactions arising from both light elementary particles and large extra dimensions can be obtained from precise force measurements between macrobodies. For electrically neutral test bodies the dominant background force at separations greater than 10^{-5} m is the gravity. At shorter separations the dominant forces are the van der Waals and Casimir forces caused by fluctuations of the electromagnetic field [20]. During the past few years a number of new experiments have been performed to measure small forces between macrobodies and to obtain stronger constraints on hypothetical long-range interactions (which are also referred to as the “fifth force” [1]). Thus, in sub-millimeter gravity experiments stronger constraints on Yukawa corrections to the Newtonian gravitational force for ranges $\sim 10^{-4}$ m and $\sim 10^{-5}$ m have been obtained [21, 22, 23, 24, 25, 26]. In a series of experiments measuring the Casimir force between gold coated test bodies the constraints on Yukawa-type interactions in a sub-micrometer range have been strengthened up to 10^4 times [27, 28, 29, 30, 31, 32, 33, 34, 35, 36, 37].

This paper exploits the results of the most precise recent determination of the Casimir pressure between two parallel gold coated plates using a micromechanical torsional oscillator. This is the third in a series of experiments using a micromechanical oscillator for precise Casimir force measurements. Results of the first two experiments were published in [36, 37] (previously a similar technique was used to demonstrate the actuation of a micromechanical device by the Casimir force [38]). A brief discussion of the results of the third experiment, and a description of the main improvements, as compared with the previous two experiments, is contained in [39]. Here we present additional experimental details related to the experiment [39] which were not discussed in the first publication, including the resistivity measurements and tests of the linearity of the oscillator used. The focus of this paper is a comparison of the experimental data with a recently proposed new theoretical approach to the thermal Casimir force [40] which is applicable to all experiments regardless of the separation between the interacting bodies. Within this framework, we first present a precise fit of the tabulated optical data [41] for the imaginary part of the dielectric permittivity of gold within a wide frequency region. The fit is obtained using a set of six oscillators representing interband transitions in gold. We then compare this fit with a previously known fit based on DESY data [42, 43]. Our theoretical approach based on the Lifshitz formula is found to be in very good agreement with the measured results. The same measured results are also compared with an alternative approach to the theory of the thermal Casimir force [44], which approach is found to be excluded by our measurements at a confidence level of 99.9%. The level of agreement between our theory and experimental data is used to set constraints on Yukawa-type corrections to Newtonian gravity originating from the exchange of light hypothetical elementary particles and/or

extra-dimensional physics. The resulting constraints are several times stronger than those derived from previous experiments. We also reanalyze constraints following [35] from experiment [30] (in [35] the confidence level of our results was not determined). As a consequence, the interaction region where the constraints from the present experiment are the strongest is widened. Special attention is paid to minor deviations between experiment and theory at the shortest separations. Although these deviations are inside the error bars and thus not statistically meaningful, we present an analysis of various explanations for them.

The plan of this paper is as follows: in Sec. 2 we present a brief description of the experimental setup and measurement results with an emphasis on novel aspects not described previously in [36, 37, 39]. Sec. 3 is devoted to the comparison of experimental data with different theoretical approaches including our new approach in [40]. The new precise oscillator fit of the optical data for gold is also presented here. Sec. 4 contains constraints on hypothetical Yukawa interactions following from the level of agreement of data with theory, and includes a comparison with constraints obtained from earlier experiments. In Sec. 5 we present our conclusions and discussion.

2 Experimental setup and measurement results

One component of our setup is an Au-coated sapphire sphere attached to an optical fiber. The thickness of the Au coating on the sphere is $\Delta_g^{(s)} = 180$ nm, and the radius of the coated sphere is $R = 151.3 \pm 0.2$ μ m. The sphere is placed at a separation z above a micromachined oscillator consisting of a heavily doped, Au-coated polysilicon plate (the thickness of the coating is $\Delta_g^{(p)} = 210$ nm) suspended at two opposite points by serpentine springs. This plate can rotate under the influence of the Casimir force $F(z)$ acting between the sphere and the plate. The rotation angle is measured by the change of the capacitance between the plate and two independently contacted polysilicon electrodes located under it (details of the setup are described in [36, 37]). The micromachined oscillator and the sphere with a fiber were mounted inside a can with magnetic damping vibration isolation, where a pressure below 10^{-4} torr was maintained.

In this experiment a dynamic measurement mode was employed. For this purpose the vertical separation between the sphere and the plate was varied harmonically, $\tilde{z}(t) = z + A_z \cos(\omega_r t)$, where ω_r is the resonant angular frequency of the oscillator in the presence of the sphere. The magnitude of the amplitude $A_z \approx 2$ nm was chosen in such a way that the oscillator exhibited a linear response. In the presence of the Casimir force $F(z)$ the resonant frequency ω_r is shifted relative to the natural angular frequency of the oscillator $\omega_0 = 2\pi \times (713.25 \pm 0.02)$ Hz determined in the absence of the sphere. In the linear regime this shift can be found using [36, 37, 38, 39]

$$\omega_r^2 = \omega_0^2 \left[1 - \frac{b^2}{I\omega_0^2} \frac{\partial F(z)}{\partial z} \right], \quad (1)$$

where b is the lever arm between the axis of plate rotation and the projection on the plate of the closest point of the sphere, I is the moment of inertia of the oscillator, and $b^2/I = (1.2432 \pm 0.0005) \mu\text{g}^{-1}$.

The actual measured quantity in this experiment is the change of the resonant frequency of the oscillator, $\omega_r - \omega_0$, under the influence of the Casimir force $F(z)$ acting between the sphere and the plate. Using (1), the experimental data for $\omega_r - \omega_0$ obtained at different separation distances can be transformed into $\partial F(z)/\partial z$. It is less useful, however, to recover the force $F(z)$ between a sphere and a plate using the force gradient. A better avenue is given by using the proximity force approximation (PFA) [45, 46, 47]

$$F(z) = 2\pi R E(z), \quad (2)$$

where $E(z)$ is the Casimir energy per unit area between two infinitely large parallel plates composed of the same materials as the sphere and the plate. Differentiating with respect to z and taking into account that the Casimir pressure between the two parallel plates is

$$P(z) = -\frac{\partial E(z)}{\partial z}, \quad (3)$$

one arrives to the expression

$$P(z) = -\frac{1}{2\pi R} \frac{\partial F(z)}{\partial z}. \quad (4)$$

From equations (1) and (4) one can immediately convert the experimental data into data for the Casimir pressure between two parallel plates. This is in fact the so-called indirect measurement [48] of the pressure. Note that in [49], where the configuration of two parallel plates was actually used in the experimental setup, the directly measured quantity was also the frequency shift due to the Casimir pressure proportional to $\partial P(z)/\partial z$. The pressure $P(z)$ was then recovered using the data for its derivative.

The calibration of absolute separations between the plate and the sphere was performed by the application of voltages in a manner analogous to that reported in [36, 37]. The use of a two-color fiber interferometer [50] and a $\approx 7\%$ improvement in vibration noise yielded an error of only 0.2 nm in a distance z_{meas} between the end of the fiber and the stationary reference. As a result, for every repetition of the Casimir pressure measurement we were able to reposition our sample to within $\Delta z_{meas} = 0.2$ nm. Finally the absolute separations z between the sphere and the plate were measured with an absolute error $\Delta z = 0.6$ nm determined at 95% confidence [37].

The indirect measurements of the Casimir pressure $P_j(z_i)$ were repeated at practically the same separations z_i ($1 \leq i \leq 293$) 33 times ($1 \leq j \leq 33$). The mean values of the experimental Casimir pressure

$$\bar{P}(z_i) = \frac{1}{33} \sum_{j=1}^{33} P_j(z_i) \quad (5)$$

are plotted in Fig. 1 as a function of separation over the entire measurement range from $z_1 = 162.03$ nm to $z_{293} =$

745.98 nm. As an example, a few mean Casimir pressures $\bar{P}(z_i)$ at different separations are presented in column (a) of Table 1. In this measurement the random experimental error is much smaller than the systematic error. Specifically, using Student's t -distribution [51] with a number of degrees of freedom $f = 32$, and choosing $\beta = 0.95$ confidence, we obtain $p = (1 + \beta)/2 = 0.975$, and $t_p(f) = 2.0$. This leads to the random experimental error

$$\Delta^{\text{rand}} P^{\text{exp}}(z_i) = s(z_i) t_p(f), \quad (6)$$

where $s(z)$ is the variance of the mean for the pressure

$$s^2(z_i) = \frac{1}{1056} \sum_{j=1}^{33} [P_j(z_i) - \bar{P}(z_i)]^2. \quad (7)$$

The random error in (6) reaches a maximum value equal to 0.46 mPa at $z = 162$ nm, decreases to 0.11 mPa at $z = 300$ nm, and maintains this value up to $z = 746$ nm.

The systematic error of the pressure measurements in this experiment is determined by the errors in the measurements of the resonance frequency, radius of the sphere (these errors were indicated above), and also by the error in using the PFA. Until 2006 the latter was not known with certainty but estimated to be of order z/R on the basis of dimensional considerations [47]. Recently, however, quantitative results on the accuracy of PFA were obtained theoretically for the configuration of a cylinder above a plate [52, 53] (the electromagnetic Casimir effect), and for a sphere above a plate [54, 55] (the scalar Casimir effect). In addition the validity of the PFA was established experimentally [56] for a sphere above a plate. In all cases at small separations the error in using the PFA was shown to be less than z/R . However, in our conservative error analysis we estimate this error with a safety margin as z/R . By combining all the above systematic errors at 95% confidence using the statistical rules described in [37], we obtain a systematic error equal to 2.12 mPa at $z = 162$ nm. The systematic error decreases to 0.44 mPa at $z = 300$ nm, and then to 0.31 mPa at $z = 746$ nm. Finally

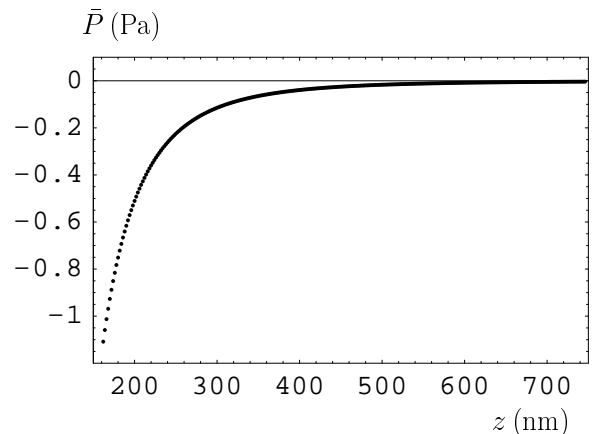


Fig. 1. Values of the mean Casimir pressure between two Au-coated plates as a function of separation.

Table 1. Magnitudes of the mean experimental Casimir pressures \bar{P} (column *a*) at different separations z compared with the magnitudes of the theoretical pressures P^{th} computed using the generalized plasma model approach (column *b*), the Leontovich surface impedance approach (column *c*), the Drude model approach (column *d*), and with the half-width, Ξ , of the 95% confidence interval for $P^{\text{th}} - \bar{P}$ (column *e*). All pressures are given in mPa.

z (nm)	<i>a</i>	<i>b</i>	<i>c</i>	<i>d</i>	<i>e</i>
162	1108.4	1098.4	1094.2	1076.2	21.2
166	1012.7	1007.1	1002.7	985.40	19.0
170	926.85	923.71	919.56	902.96	17.1
180	751.19	750.58	747.06	732.14	13.3
190	616.00	616.71	613.70	600.28	10.5
200	510.50	511.26	508.70	496.62	8.40
250	225.16	225.71	224.45	217.11	3.30
300	114.82	114.87	114.18	109.48	1.63
350	64.634	64.574	64.176	61.004	0.98
400	39.198	39.096	38.850	36.617	0.69
450	25.155	25.034	24.874	23.247	0.54
500	16.822	16.785	16.678	15.456	0.47
550	11.678	11.669	11.595	10.654	0.42
600	8.410	8.365	8.312	7.573	0.39
650	6.216	6.151	6.113	5.522	0.38
700	4.730	4.626	4.598	4.118	0.36
746	3.614	3.620	5.598	3.198	0.35

we combine the resulting random and systematic errors at a 95% confidence to arrive at the total experimental error, $\Delta^{\text{tot}} P^{\text{exp}}(z)$, approximately equal to the systematic error at all separations considered. Detailed information on the statistical methods used in our error analysis can be found in [37,48]. As a result, the total relative experimental error $\Delta P^{\text{exp}}(z)/|\bar{P}(z)|$ varies from 0.19% at $z = 162$ nm, to 0.9% at $z = 400$ nm, and to 9.0% at $z = 746$ nm. Hence this is the most precise experiment on the Casimir effect performed up to date.

Several additional measurements and tests were performed in order to compare the experimental data with theory in a conclusive manner. In order to include the effects of surface roughness in theoretical computations of the Casimir pressure we have investigated the topography of the metallic coatings both on the plate (*p*) and on the sphere (*s*) using an AFM probe in tapping mode. All AFM scans were squares with sizes ranging from $0.5 \times 0.5 \mu\text{m}$ to $10 \times 10 \mu\text{m}$. The information obtained was indistinguishable. In the case of a sphere the surface curvature was taken into account. For this purpose the image was planarized, and then the roughness analysis performed. For a typical scan of $5 \times 5 \mu\text{m}$ the effect of curvature is about 40 nm. From AFM images of the surfaces, the fraction of each surface area $v_i^{(p,s)}$ with height $h_i^{(p,s)}$ was determined. It was found that for the sphere ($1 \leq i \leq K^{(s)} = 106$) $h_i^{(s)}$ varies from 0 to 10.94 nm and for the plate ($1 \leq i \leq K^{(p)} = 85$) $h_i^{(p)}$ varies from 0 to 18.35 nm. Here, the highest peaks on the sphere and on the plate are almost

of the same height as in the previous experiment of [37] (11.06 nm and 20.65 nm on the sphere and plate, respectively [37]). However, they are much lower than the highest peaks in the experiment [36]. The respective zero roughness levels on the sphere and on the plate, $H_0^{(s)}$ and $H_0^{(p)}$, are found from

$$\sum_{i=1}^{K^{(p,s)}} \left[H_0^{(p,s)} - h_i^{(p,s)} \right] v_i^{(p,s)} = 0. \quad (8)$$

From (8) using the roughness data one obtains $H_0^{(s)} = 5.01$ nm and $H_0^{(p)} = 9.66$ nm. Note that precise measurements of absolute separations z discussed above result in separations just between the zero roughness levels determined in (8).

Special tests were performed to investigate possible nonlinear behavior of the oscillator under the influence of the Casimir force. First, the resonance frequency ω_r observed under the excitation leading to a harmonically varying separation with amplitude A_z was compared with the resonance frequency with no excitation (i.e., with separation varied just through the thermal noise). When the amplitude A_z was less than 4 nm, no deviation was observed between the measured resonance frequency and the thermal resonance frequency within the ≈ 5 mHz noise. This was performed at different separations (recall that the amplitude actually used in the experiment was $A_z \approx 2$ nm). The value of A_z^{cr} at which deviations are observed is a function of separation. For example, at $z = 199.8$ nm $A_z^{cr} = 4.5$ nm, at $z = 247.3$ nm $A_z^{cr} = 10.0$ nm, and at $z = 302.4$ nm, $A_z^{cr} = 15.0$ nm. In all cases, when observed, nonlinearities decrease the resonance frequency.

Another test performed was a check for the strength of the signal at different harmonics of the excitation. The experiment was done with the excitation $\tilde{z}(t)$ at the resonant frequency ω_r . The checks were performed with the excitations at frequencies $2\omega_r$ and $\omega_r/2$, but no change in the response at ω_r was observed for $A_r < 4$ nm. For larger amplitudes the results were consistent with what was observed in the first test. These tests all verify that

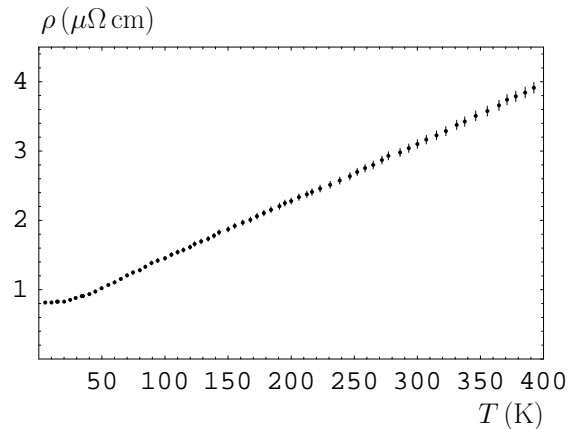


Fig. 2. Resistivity of the Au films (measured with an error of about 2%) as a function of temperature.

the oscillator was in fact operating in a linear regime for our measurements.

It is significant that the comparison of experimental data with theory of the Casimir force requires knowledge of the optical and electronic parameters of the Au layers. In previous experiments all of these parameters, including the plasma frequency ω_p and relaxation parameter $\gamma(T)$, were taken from tables [41]. For a more conclusive comparison of this experiment with different theoretical approaches, we measured the resistivity ρ of the Au films as a function of temperature in the region from $T_1 = 3$ K to 400 K. These measurements were performed using a four probe approach on Au films of the same thickness which were deposited at the same time as the Au deposition on the oscillator, and on the same substrates. The samples were approximately 1 mm long and 10 μm wide. The resistivity of each sample was found by taking into account its geometrical factor with an error of about 2% arising from the errors in measuring of the sample's geometry. The experimental data for the resistivity versus temperature are presented in Fig. 2. These data at $T \gg T_D/4$ (where $T_D = 165$ K is the Debye temperature for Au) were fitted to a straight line [57]

$$\rho(T) = \frac{4\pi}{\omega_p^2 \tau(T)} = \frac{4\pi v_F}{\omega_p^2 l(T)} = \frac{CT}{\omega_p^{3/2}}. \quad (9)$$

Here $\tau(T) = l(T)/v_F$ is the relaxation time, $l(T) \sim T$ is the mean free path of an electron, $v_F \sim \omega_p^{1/2}$ is the Fermi velocity, and $C = \text{const.}$ The fit results in $C/\omega_p^{3/2} = (8.14 \pm 0.16) \text{ n}\Omega \text{ cm K}^{-1}$. On the other hand, using the resistivity data for pure Au as a function of temperature [58] and the previously used value of the plasma frequency $\tilde{\omega}_p = 9.0 \text{ eV}$ [41, 59] we obtain $C/\tilde{\omega}_p^{3/2} = 8.00$. As a result we find for the Au film used in our experiment $\omega_p = (8.9 \pm 0.1) \text{ eV}$. Here, the absolute error of 0.1 eV arises from the errors of the resistivity measurements. Some of the theoretical approaches to the thermal Casimir force require a knowledge of the relaxation parameter. The smooth Drude extrapolation of the imaginary part of the Au dielectric permittivity, given by the tabulated optical data [41], yields the relaxation parameter at room temperature $\gamma = 0.0357 \text{ eV}$ (which compares with $\tilde{\gamma} = 0.035 \text{ eV}$ used in previous work [36, 37, 59]).

3 Comparison of experimental data with different theoretical approaches to the thermal Casimir force

The theoretical description of both the van der Waals and Casimir pressures between planar plates at temperature T in thermal equilibrium is given by the Lifshitz formula [60]

$$P(z) = -\frac{k_B T}{\pi} \sum_{l=0}^{\infty} \left(1 - \frac{1}{2} \delta_{l0}\right) \int_0^{\infty} k_{\perp} dk_{\perp} q_l + \left[r_{\text{TM}}^{-2}(\xi_l, k_{\perp}) e^{2q_l z} - 1 \right]^{-1} \quad (10)$$

$$+ \left[r_{\text{TE}}^{-2}(\xi_l, k_{\perp}) e^{2q_l z} - 1 \right]^{-1} \Big\}.$$

Here $k_{\perp} = |\mathbf{k}_{\perp}|$ is the magnitude of the wave vector component in the plane of the plates, $q_l^2 = k_{\perp}^2 + \xi_l^2/c^2$, $\xi_l = 2\pi k_B T l / \hbar$ are the Matsubara frequencies, $l = 0, 1, 2, \dots$, δ_{lm} is Kronecker's delta symbol, and k_B is the Boltzmann constant. The reflection coefficients for two independent polarizations of the electromagnetic field (the transverse magnetic and transverse electric) are defined as

$$r_{\text{TM}}(\xi_l, k_{\perp}) = \frac{\varepsilon_l q_l - k_l}{\varepsilon_l q_l + k_l}, \quad r_{\text{TE}}(\xi_l, k_{\perp}) = \frac{k_l - q_l}{k_l + q_l}, \quad (11)$$

where

$$k_l = \sqrt{\varepsilon_l \frac{\xi_l^2}{c^2} + k_{\perp}^2}, \quad \varepsilon_l = \varepsilon(i\xi_l), \quad (12)$$

and $\varepsilon(\omega)$ is the frequency-dependent dielectric permittivity of the plates.

Note that (10) is the expression for a plate of infinite thickness. Using the Lifshitz formula for layered structures [47], it is easy to see that for Au layer thicknesses larger than 150 nm (as in our case) at, e.g., $z = 400$ nm the error due to the replacement of a layer with a semispace is less than 0.003%.

It is known that there is some controversy concerning the application of (10), (11) to real metals. These controversies arise from different approaches to the calculation of the zero-frequency ($l = 0$) term in (10). For real materials (Au for instance) $\varepsilon(i\xi_l)$ is usually found through the Kramers-Kronig relation

$$\varepsilon(i\xi_l) = 1 + \frac{1}{\pi} \text{P} \int_{-\infty}^{\infty} \frac{\omega \varepsilon''(\omega)}{\omega^2 + \xi_l^2} d\omega, \quad (13)$$

where $\varepsilon''(\omega)$ is the imaginary part of the dielectric permittivity and the integral is taken as a principal value. Optical data for $\varepsilon''(\omega)$ are available within some restricted frequency region [41], and it is common to smoothly extrapolate available data to lower frequencies using the imaginary part of the Drude model dielectric permittivity

$$\varepsilon''(\omega) = \frac{\omega_p^2 \gamma}{\omega(\omega^2 + \gamma^2)}. \quad (14)$$

If such an extrapolation is performed down to lower frequencies, including zero frequency [44], the use of the resulting $\varepsilon(i\xi_l)$ in the Lifshitz theory leads to a violation of the Nernst heat theorem for perfect crystal lattices [61], and the Casimir pressures calculated using (10) are in contradiction with experiment [36, 37, 39]. Because of this, two other approaches to the determination of $\varepsilon(i\xi_l)$ were proposed in the literature. According to the plasma model approach [62, 63], the tabulated optical data are not used and $\varepsilon(i\xi_l)$ is found from the free electron plasma model

$$\varepsilon(i\xi_l) = 1 + \frac{\omega_p^2}{\xi_l^2}. \quad (15)$$

According to the impedance approach [64, 65], the reflection coefficients (11) are expressed in terms of the Leontovich surface impedance $Z(\omega)$ instead of the dielectric

permittivity. The contributions of all Matsubara frequencies with $l \geq 1$ are obtained from tabulated optical data extrapolated by the Drude model using a relation $Z(i\xi_l) = 1/\sqrt{\varepsilon(i\xi_l)}$. This leads to approximately the same calculation results as the use of the dielectric permittivity. As to the contribution of zero Matsubara frequency, it is obtained using the impedance of infrared optics, and is different from that obtained using the Drude model (a discussion of different approaches can be found in [66,67]). Note that the impedance approach was used for the first comparison of the measurement data of this experiment with theory [39].

Although the plasma model and impedance approaches are in agreement with thermodynamics, neither can be considered as universally valid. The plasma model approach completely neglects dissipation. Because of this, it is in agreement with measured data only for experiments [36,37,39] performed at separations larger than the plasma wavelength λ_p . As for the impedance approach, it is not applicable to short-separation experiments [30] because when $z < \lambda_p$ the Leontovich impedance boundary conditions become invalid due to the violation of the inequality $|Z(\omega)| \ll 1$.

Recently [40] a new approach to the thermal Casimir force between real metals was proposed which is equally applicable at both small and large separations. This approach is based on the use of the generalized plasma-like dielectric permittivity

$$\varepsilon(\omega) = 1 - \frac{\omega_p^2}{\omega^2} + \sum_{j=1}^K \frac{f_j}{\omega_j^2 - \omega^2 - ig_j\omega}, \quad (16)$$

which takes into account the interband transitions of core electrons. Here $\omega_j \neq 0$ are the resonant frequencies of the core electrons, g_j are the respective relaxation frequencies, f_j are the oscillator strengths, and K is the number of oscillators. Note that the term $-\omega_p^2/\omega^2$ on the right-hand side of (16) describes free electrons and leads to a purely imaginary current. This contribution to $\varepsilon(\omega)$ is entirely real and does not include dissipation. Importantly, the oscillator term on the right-hand side of (16) does not include the oscillator with zero resonant frequency $\omega_0 = 0$, which is equivalent to the Drude dielectric function, i.e., it does not describe conduction electrons but only core electrons. This term incorporates dissipation due to interband transitions.

In [40] the Lifshitz theory together with the dielectric permittivity (16) was used to calculate the thermal Casimir force in a short-separation experiment [30], and the experimental results were found to be in good agreement with theory. For this purpose the oscillator parameters of Au in (16) were taken from [42,43] where they were found using the 3-oscillator model fitted to old DESY data. Below we compare the 3-oscillator fit of [42,43] with the more complete data set of [41] and perform a more exact 6-oscillator fit. The resulting oscillator parameters are used to calculate the Casimir pressure in the most precise experiment described in the previous section.

The Kramers-Kronig relation (13) was derived [68] for dielectric permittivities which were regular or which had a first order pole at zero frequency. For the dielectric permittivity (16) which has a second order pole at $\omega = 0$, the Kramers-Kronig relation expressing $\varepsilon(i\omega)$ in terms of $\varepsilon''(\omega)$ is the following [40]:

$$\varepsilon(i\xi_l) = 1 + \frac{1}{\pi} \text{P} \int_{-\infty}^{\infty} \frac{\omega \varepsilon''(\omega)}{\omega^2 + \xi_l^2} d\omega + \frac{\omega_p^2}{\xi_l^2}. \quad (17)$$

In the tables of [41] the most complete data are collected for real, $n_1(\omega)$, and imaginary, $n_2(\omega)$, parts of the complex refractive index of Au in the frequency region from 0.125 eV to 9919 eV ($1 \text{ eV} = 1.519 \times 10^{15} \text{ rad/s}$). From these data, the imaginary part of the Au dielectric permittivity is expressed as $2n_1(\omega)n_2(\omega)$. To obtain the contribution of core electrons to the dielectric permittivity, we consider the difference

$$\varepsilon''_{Au}(\omega) = 2n_1(\omega)n_2(\omega) - \frac{\tilde{\omega}_p^2 \tilde{\gamma}}{\omega(\omega^2 + \tilde{\gamma}^2)}, \quad (18)$$

where in accordance with (14) the subtracted term approximately describes the contribution of free conduction electrons to optical data. In Fig. 3 the quantity ε''_{Au} is plotted as a function of ω within the frequency region from 2.0 eV to 25 eV (solid line). For $\omega < 2 \text{ eV}$ the dielectric permittivity is determined by free conduction electrons, and for $\omega > 2.5 \text{ eV}$ there is already practically no contribution from conduction electrons, and $\varepsilon''_{Au}(\omega) \approx 2n_1(\omega)n_2(\omega)$. The upper limit of the region under consideration is determined by the frequencies contributing to the Casimir pressure (10). Even at the shortest separation considered, $z = 160 \text{ nm}$, the characteristic frequency $\Omega_c = c/(2a) \approx 0.62 \text{ eV}$. Bearing in mind that even for precise computations of the pressure it is sufficient to take into account the contribution from Matsubara frequencies up to $15\Omega_c$, setting the upper limit of our region equal to 25 eV is more than adequate.

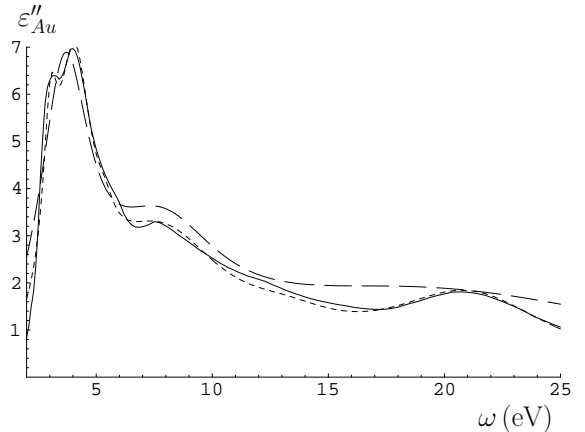


Fig. 3. Tabulated optical data for the imaginary part of Au dielectric permittivity [41] (with the contribution of conduction electrons subtracted) are shown by the solid line. The oscillator fits are shown as long-dashed line [42,43] (DESY data, 3 oscillators) and as short-dashed line (6 oscillators).

The solid line in Fig. 3 was fitted to the imaginary part of dielectric permittivity (16)

$$\varepsilon''(\omega) = \sum_{j=1}^K \frac{f_j g_j \omega}{(\omega_j^2 - \omega^2)^2 + g_j^2 \omega^2} \quad (19)$$

with $K = 6$ oscillators. The resulting set of oscillator parameters f_j , ω_j and g_j is presented in Table 2. In Fig. 3 the imaginary part of permittivity calculated using the analytic expression (19) is shown by the short-dashed line. In the same figure the 3-oscillator fit from [42,43] is shown as the long-dashed line. As is seen in Fig. 3, the short-dashed line based on the 6-oscillator fit better reproduces the actual data than does the long-dashed line using the 3-oscillator fit.

Table 2. The oscillator parameters for Au in equations (16) and (19) found here from the 6-oscillator fit to the tabulated optical data in [41].

j	ω_j (eV)	g_j (eV)	f_j (eV ²)
1	3.05	0.75	7.091
2	4.15	1.85	41.46
3	5.4	1.0	2.700
4	8.5	7.0	154.7
5	13.5	6.0	44.55
6	21.5	9.0	309.6

The Casimir pressure $P_L(z)$ at all separations of interest was computed using the Lifshitz theory in equations (10)–(12) and (16) with $\omega_p = 8.9$ eV, as determined for our films in Sec. 2, and the oscillator parameters from Table 2. For comparison with the experimental data, the values of $P_L(z)$ were geometrically averaged over all possible separations between the rough surfaces weighted with the fractions of the total area occupied by each separation, as discussed in Sec. 2. This results in the theoretical Casimir pressures taking surface roughness into account via the equation

$$P^{\text{th}}(z_i) = \sum_{k=1}^{K^{(s)}} \sum_{j=1}^{K^{(p)}} v_k^{(s)} v_j^{(p)} \times P_L \left(z_i + H_0^{(s)} + H_0^{(p)} - h_k^{(s)} - h_j^{(p)} \right). \quad (20)$$

The pressures $P^{\text{th}}(z_i)$ were computed at each experimental point z_i . Note that (20) takes into account the combined (nonmultiplicative) effect of nonzero temperature and finite conductivity on the one hand [this is incorporated in $P_L(z)$ computed using the Lifshitz formula], and of surface roughness on the other. The contributions of diffraction-type and correlation effects in the roughness correction [69,70], which are not taken into account in the geometrical averaging (20), were shown to be negligible [37]. In this experiment the contribution of the roughness

correction to the Casimir pressure computed using (20) is very small. For example, at $z = 162$ nm the roughness correction contributes only 0.52% of the total pressure. At separations $z = 170, 200$ and 350 nm roughness contributes only 0.48, 0.35 and 0.13% of the Casimir pressure, respectively. The magnitudes of the computed theoretical Casimir pressures at some experimental separations are listed in column (b) of Table 1.

We now discuss the accuracy of our computations. One of the sources of the theoretical errors is the sample-to-sample variation of the optical data for the complex index of refraction. As was shown in [37] (see also [30]), in our experiments the variation of the optical data leads to an uncertainty in the magnitude of the Casimir pressure which is substantially smaller than 0.5%. To be conservative, we admit an uncertainty as large as 0.5% in the computations due to the use of tabulated optical data over the entire measurement range. There are claims in the literature [71] that the theoretical computations of the Casimir pressure between gold surfaces are burdened by up to 5% errors due to the use of different Drude parameters measured and calculated for different samples. This is, however, irrelevant to our experiment. The hypothesis that the magnitude of ω_p is much smaller than the value we have used above (i.e., $\omega_p = 6.85$ eV or 7.50 eV, as suggested in [71]) is rejected at high confidence by our experiment, and by all previously performed measurements of the Casimir force between Au surfaces.

The other possible source of theoretical errors is connected with the fact that we compute the Casimir pressure at experimental separations which are determined with an error $\Delta z = 0.6$ nm [72]. Noting that the dominant theoretical dependence of the Casimir pressure is z^{-4} , one finds that the relative error in the pressure is equal to $4\Delta z/z$. This varies from 1.5% at $z = 160$ nm to 0.32% at $z = 750$ nm. The other theoretical errors, e.g., arising from neglect of patch potentials or spatial nonlocality, were analyzed in detail in [37] and found to be negligible. By combining the above two theoretical errors discussed here and in the previous paragraph at a 95% confidence level using the statistical procedure applicable to systematic errors described by a uniform distribution [37,48], we obtain the total theoretical error $\Delta^{\text{tot}} P^{\text{th}}(z)$ as a function of separation. This error assumes a maximum value of 18.7 mPa at $z = 162$ nm, which is almost 9 times larger than the total experimental error. Note that in a similar analysis in [37], one additional theoretical error due to the use of PFA was included. In [37] it was first combined with the theoretical error due to sample-to-sample variation of the optical data, with the result that the distribution law of the combined quantity was not uniform. In this work, however, the error due to the accuracy of PFA is included with the experimental errors. Because of this, the total theoretical error is determined by only two contributions. With the increase of separation to $z = 300, 400$ and 746 nm, the total theoretical error decreases to 1.15, 0.34 and 0.024 mPa, respectively. The relative theoretical error $\Delta P^{\text{th}}(z)/|P^{\text{th}}(z)|$ assumes a maximum value of 1.7% at $z = 162$ nm. When the separation increases

to $z = 300, 400$ and 746 nm, the relative theoretical error decreases to 1.0, 0.86 and 0.65%, respectively. This is mainly explained by the decreased role of uncertainty in determining the separations.

We can now compare experiment and theory by considering the differences $P^{\text{th}}(z_i) - \bar{P}(z_i)$ at each experimental separation z_i . The confidence interval for the quantity $P^{\text{th}}(z_i) - \bar{P}(z_i)$ determined at 95% confidence probability is given by $[-\Xi_{0.95}(z_i), \Xi_{0.95}(z_i)]$ where the half-width of this interval can be found using the composition rule [37, 48]

$$\Xi_{0.95}(z_i) = \min \left\{ \Delta^{\text{tot}} P^{\text{th}}(z_i) + \Delta^{\text{tot}} P^{\text{exp}}(z_i), k_{0.95}^{(2)} \sqrt{[\Delta^{\text{tot}} P^{\text{th}}(z_i)]^2 + [\Delta^{\text{tot}} P^{\text{exp}}(z_i)]^2} \right\}. \quad (21)$$

Here for two composed quantities $k_{0.95}^{(2)} = 1.1$. The values of the half-width of the confidence interval are listed in the last column of Table 1.

In Fig. 4a the differences $P^{\text{th}}(z_i) - \bar{P}(z_i)$ at all experimental points are shown as dots. In the same figure the confidence interval $[-\Xi_{0.95}(z_i), \Xi_{0.95}(z_i)]$ at each z is situated between the solid lines. As seen in the figure, all dots (and not only 95% of them as required by the rules of mathematical statistics) are well inside the confidence interval at all separations considered. This means that the experimental data are consistent with theory based on the generalized plasma-like dielectric permittivity (16), and that in our conservative error analysis the errors (especially at short separations) are overestimated. For comparison purposes in Fig. 4b we plot as dots the differences $\tilde{P}^{\text{th}}(z_i) - \bar{P}(z_i)$ where the experimental data are the same as in Fig. 4a, but with $\tilde{P}^{\text{th}}(z_i)$ computed as in [39] using the Leontovich surface impedance approach, with the Drude parameters $\omega_p = 8.9$ eV, $\gamma = 0.0357$ eV. In Table 1, column (c) we present the magnitudes of the Casimir pressures $\tilde{P}^{\text{th}}(z_i)$ computed using the surface impedance approach at different separations. As is seen in Fig. 4b, the impedance theoretical approach is also consistent with the data. However, while in Fig. 4a there are practically no deviations between experiment and theory at $z > 350$ nm, in Fig. 4b the deviations are noticeable up to $z = 450$ nm. By comparing columns (b) and (c) in Table 1, we can conclude that the differences between the two theoretical approaches do not exceed the magnitude of the theoretical error. The comparison of columns (b) and (c) with column (a) shows that at all separations the approach using the generalized plasma-like model is in somewhat better agreement with data than the surface impedance approach. As is seen in Fig. 4a,b, the largest deviations between both theoretical approaches and experimental data are at short separations from 162 to 200 nm. Although these deviations are not statistically meaningful, because they are well inside the confidence interval, in Sec. 5 we will discuss possible reasons leading to the deviations between experiment and theory at shortest separations.

A completely different situation occurs when we compare the experimental data with the alternative approach to the thermal Casimir force [44] using the Drude model

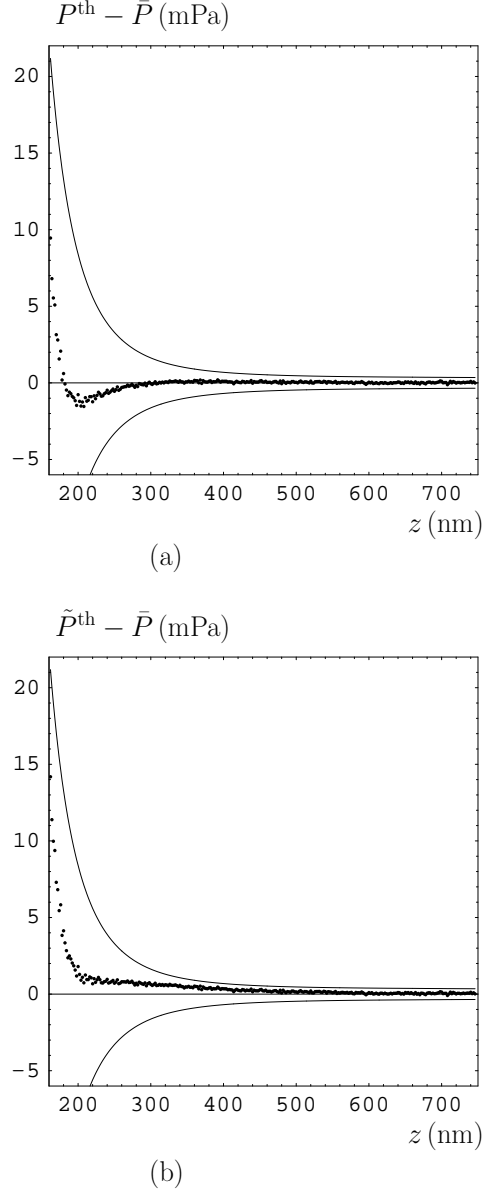


Fig. 4. Differences between theoretical Casimir pressures computed using the generalized plasma model approach (a) and the Leontovich surface impedance approach (b) and mean experimental Casimir pressures (dots) versus separation. Solid lines indicate the limits of the 95% confidence intervals.

to compute the contribution of the zero-frequency term in the Lifshitz formula. To perform the comparison, we calculate the theoretical Casimir pressures in the framework of [44] with the refined values of the Drude parameters $\omega_p = 8.9$ eV, $\gamma = 0.0357$ eV (all details of this approach and of computations can be found in [37]). The magnitudes of the resulting Casimir pressures P_D^{th} at a few different separations are listed in Table 1, column (d). In Fig. 5 we plot the differences $P_D^{\text{th}}(z_i) - \bar{P}(z_i)$ at all experimental separations. The confidence interval $[-\Xi_{0.95}(z_i), \Xi_{0.95}(z_i)]$

at each z_i is the same for all theoretical approaches. Once again, the limits of the confidence interval are denoted by the solid lines (in Fig. 5 only one solid line is shown because practically all dots are above it). As is seen in Fig. 5, the Drude model theoretical approach is experimentally excluded at a 95% confidence level within the whole measurement range from 162 to 746 nm. This conclusion is confirmed by the calculation data in Table 1. Subtracting the magnitudes of the theoretical Casimir pressures, $|P_D^{\text{th}}|$, in column (d) from the experimental results, $|\bar{P}|$, in column (a), we obtain at all separations larger results than the half-width of the confidence interval, $\Xi_{0.95}(z)$, given in column (e).

The wide gaps between the solid line and dots in Fig. 5 suggest that the Drude model approach is actually excluded experimentally at an even higher confidence than 95%. To make this argument quantitative, we calculate the half-width of a confidence interval at 99.9% confidence from

$$\frac{\Xi_{0.999}(z)}{\Xi_{0.95}(z)} = \frac{t_{(1+0.999)/2}(32)}{t_{(1+0.95)/2}(32)} \approx 1.85, \quad (22)$$

where $t_p(f)$ is the Student coefficient used in Sec. 2. The limits of the 99.9% confidence intervals obtained in (22) are shown in Fig. 5 by the dashed line. As is seen in Fig. 5, the differences $P_D^{\text{th}} - \bar{P}$ are found outside of the 99.9% confidence interval at separations from 210 to 620 nm. This conclusively demonstrates that our experiment is irreconcilable with the Drude model approach to the thermal Casimir force. At the same time, the approaches based on the generalized plasma-like dielectric permittivity, and on the Leontovich surface impedance, are consistent with experiment. Note that in our experiment the Drude model approach is excluded at separations below $1 \mu\text{m}$. In the proposed experiments [73,74,75] it is planned to test the predictions of different theoretical approaches to the ther-

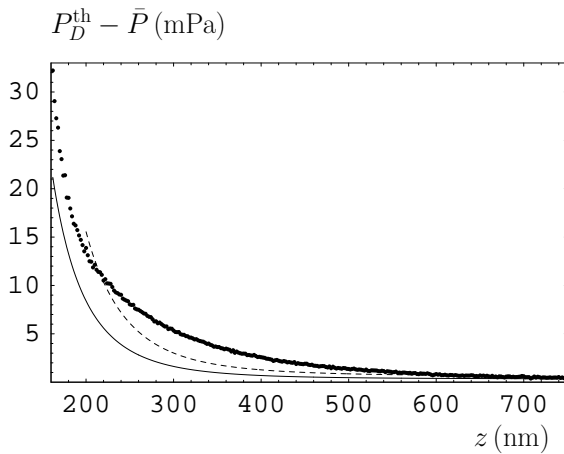


Fig. 5. Differences between theoretical Casimir pressures computed using the Drude model approach and mean experimental Casimir pressures (dots) versus separation. The solid line indicates the limits of the 95% confidence intervals while the dashed line indicates the limits of the 99.9% confidence intervals.

mal Casimir force at separations of about several micrometers.

4 Constraints on Yukawa-type hypothetical interactions and light elementary particles

As was mentioned in the Introduction, at separations between macroscopic bodies of about $1 \mu\text{m}$ and less, the Casimir force is the dominant background force. From the level of agreement between the experimental data for the Casimir pressure and Lifshitz theory (with a generalized plasma-like permittivity in Sec. 3), one can constrain any additional force which may coexist with the Casimir force. As noted in the Introduction, many extensions of the standard model predict a Yukawa correction to the Newtonian potential energy between two point masses m_1 and m_2 at a separation r , given by [10,14,15]

$$V(r) = -\frac{Gm_1m_2}{r} \left(1 + \alpha e^{-r/\lambda}\right). \quad (23)$$

Here G is the Newtonian gravitational constant, α is a dimensionless constant characterizing the strength of the Yukawa interaction, and λ is its range.

The total force acting between two parallel plates due to the potential (23) can be obtained by integration of (23) over the volumes of the plates, and subsequent negative differentiation with respect to z . In experiments measuring the Casimir force the contribution of the gravitational force is very small and can be neglected [35,36]. Thus, in what follows we consider only the contribution from the Yukawa term in (23).

To find the Yukawa pressure for our setup we should take into account the detailed structure of our test bodies. (As was shown in Sec. 3, for the calculation of the Casimir pressure it is possible to replace the Au coating films with Au semispaces and we need not consider the underlying substrate.) In the present experiment a sapphire sphere of density $\rho_s = 4.1 \text{ g/cm}^3$ was first coated with a layer of Cr of density $\rho_c = 7.14 \text{ g/cm}^3$ and thickness $\Delta_c = 10 \text{ nm}$, and then with an external layer of gold of thickness $\Delta_g^{(s)} = 180 \text{ nm}$ and density $\rho_g = 19.28 \text{ g/cm}^3$. The Si plate of thickness $L = 3.5 \mu\text{m}$, and density $\rho_{Si} = 2.33 \text{ g/cm}^3$ was also first coated with a layer of Cr of $\Delta_c = 10 \text{ nm}$ thickness, and then with a layer of gold of $\Delta_g^{(p)} = 210 \text{ nm}$ thickness. Under the conditions $z, \lambda \ll R$, satisfied in this experiment, the equivalent Yukawa pressure between the two parallel plates with the same layer structure as the above sphere and a plate is given by [32,47]

$$P^{\text{hyp}}(z) = -2\pi G\alpha\lambda^2 e^{-z/\lambda} \quad (24) \\ \times \left[\rho_g - (\rho_g - \rho_c)e^{-\Delta_g^{(s)}/\lambda} - (\rho_c - \rho_s)e^{-(\Delta_g^{(s)} + \Delta_c)/\lambda} \right] \\ \times \left[\rho_g - (\rho_g - \rho_c)e^{-\Delta_g^{(p)}/\lambda} - (\rho_c - \rho_{Si})e^{-(\Delta_g^{(p)} + \Delta_c)/\lambda} \right].$$

We have verified that the surface roughness, as reported in Sec. 2, cannot significantly affect the magnitude of a hypothetical pressure with an interaction range longer than

10 nm, and hence can be neglected. Because of this, there is no need to perform geometrical averaging as in (20) when calculating the Yukawa interaction.

According to Sec. 3, theories of the thermal Casimir force using the generalized plasma-like permittivity or the Leontovich surface impedance are consistent with experimental data. As was noted in Sec. 3, in our conservative analysis the errors [and consequently the width of the confidence interval $2\tilde{\Xi}(z)$] are overestimated. The reason for this is that we have included the error due to the uncertainty of experimental separations Δz in the analysis of the theoretical errors. As a result, the theoretical pressures acquired an extra error of $\approx 4\Delta z/z$ which led to enormous widening of the confidence interval at short separations (see Figs. 4 and 5). This approach was useful in selecting among different theories of the thermal Casimir force, and permitted us to exclude the one based on the use of the Drude model at practically 100% confidence. However, as is clearly seen in Fig. 4a,b, the actual width of the confidence interval is much less than that between the solid lines (recall that the actual confidence interval determined at 95% confidence should contain about 95% of the data dots but not all of them). It is easily seen that if the theoretical error $4\Delta z/z$ due to uncertainties in experimental separations is disregarded, the resulting more narrow confidence interval $[-\tilde{\Xi}(z), \tilde{\Xi}(z)]$ still contains all dots representing $P^{\text{th}}(z) - \bar{P}(z)$ within the separation region from 180 to 746 nm. At a separation $z = 180$ nm, the half-width $\tilde{\Xi} = 4.80$ mPa. At typical separations $z = 200, 250, 300, 350, 400$ and 450 nm $\tilde{\Xi}$ is equal to 3.30, 1.52, 0.84, 0.57, 0.45 and 0.40 mPa, respectively. Thus, for $180 \text{ nm} \leq z \leq 746 \text{ nm}$ the magnitude of the hypothetical pressure should satisfy the inequality

$$|P^{\text{hyp}}(z)| \leq \tilde{\Xi}(z). \quad (25)$$

Bearing in mind that the half-width of the confidence interval $\tilde{\Xi}(z)$ was defined at a 95% confidence, the same confidence also applies to the constraints following from the inequality (25).

We have performed a numerical analysis of equations (24) and (25) at different separations and determined the resulting region of (λ, α) -plane where the inequality (25) is satisfied, so that the existence of Yukawa interaction is consistent with the level of agreement achieved between data on the measurement of the Casimir force and relevant theory. The strongest constraints within the interaction region $10 \text{ nm} \leq \lambda \leq 56 \text{ nm}$ are obtained from the comparison of measurements with theory at a separation $z = 180$ nm. With the increase of λ , the strongest constraints on α were obtained from the consideration of larger separations. Thus constraints in the regions $56 \text{ nm} \leq \lambda \leq 71 \text{ nm}$, $71 \text{ nm} \leq \lambda \leq 89 \text{ nm}$, $89 \text{ nm} \leq \lambda \leq 140 \text{ nm}$, $140 \text{ nm} \leq \lambda \leq 220 \text{ nm}$ and $220 \text{ nm} \leq \lambda \leq 500 \text{ nm}$ were obtained from the agreement between Casimir pressure measurements and theory at separations $z = 200, 250, 300, 350$ and 400 nm, respectively.

The resulting constraints on α are plotted in Fig. 6 for different values of λ (line 1). The region in the (λ, α) -plane above the line 1 is excluded by the results of the Casimir

pressure measurements compared with theory, and below line 1 is allowed. For comparison, constraints from earlier experiments are also shown in Fig. 6 in a similar manner.

Special attention should be paid to line 2 representing constraints following from the short-separation experiment [30] on the measurement of the Casimir force between an Au-coated sphere and a plate using an atomic force microscope. The constraints on a Yukawa hypothetical interaction following from that experiment were obtained in [35], and later used in [36,37,39] for comparison with constraints following from other experiments. However, in [35] the level of agreement between experiment and theory at zero temperature was described in terms of the root-mean-square deviation which, as was recognized later in [37], is not an appropriate quantity in strongly nonlinear situations. In addition, the calculational scheme using the root-mean-square deviation does not permit us to determine the confidence level of the results.

Here we reanalyze the experimental data of [30] and compare them with theory using the Lifshitz formula at laboratory temperatures in a sphere-plate configuration, supplemented by the generalized plasma-like dielectric permittivity (16). The results of this reanalysis are expressed in terms of the confidence interval $[-\Theta(z), \Theta(z)]$ determined at 95% confidence for the differences between theoretical and mean experimental Casimir forces, $F^{\text{th}}(z) - \bar{F}(z)$. This interval includes, in particular, the theoretical

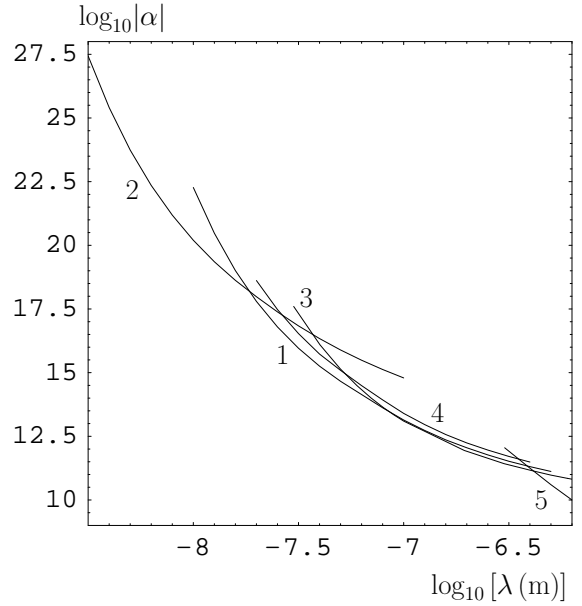


Fig. 6. Constraints on the strength of the Yukawa interaction versus interaction range. Line 1 is obtained in this paper, line 2 was obtained in [35] using the Casimir force measurement of [30] and adapted in this paper to the accepted 95% confidence level. Lines 3 and 4 were obtained in [78] and [37], respectively. Line 5 was obtained in the first reference of [32] using the Casimir force measurement [27]. The region of the (λ, α) plane above each line is excluded and below the line is allowed.

errors $3\Delta z/z$ arising due to uncertainties of experimental separations in the sphere-plate configuration. This interval cannot be narrowed as we did above in the case of the present experiment, because the measurement in [30] is inherently noisier. For example, at $z = 61.08$ nm the half-width of the confidence interval is $\Theta = 31.6$ pN, and with an increase of separation up to 100.15 and 200.46 nm it decreases to 9.17 and 7.20 pN, respectively. The resulting constraints at a 95% confidence level are determined from

$$|F^{\text{hyp}}(z)| \leq \Theta(z), \quad (26)$$

where $F^{\text{hyp}}(z)$ is the Yukawa hypothetical force acting between an Au coated sphere and a plate [35,36]. These constraints are represented by line 2 in Fig. 6. Note that the constraints given by line 2 are up to order of magnitude weaker than those in [35], but they benefit from high confidence, and can be compared with future work on the subject by using the same rigorous approach to the comparison experiment with theory as proposed in [37,76,77].

The other lines in Fig. 6 are obtained from the Casimirless experiment [78] (line 3), previous measurements of the Casimir pressure using the micromachined oscillator [37] (line 4), and in [32] (the first paper) from a torsion pendulum experiment [27] (line 5). As is seen in Fig. 6, the resulting constraints represented by line 1 are strongest within the interaction range $20 \text{ nm} \leq \lambda \leq 86 \text{ nm}$ with the largest improvement by a factor 4.4 at 26 nm. Note that further strengthening of the resulting constraints on α within a submicrometer interaction range could provide important information concerning predicted particles such as scalar axions, graviphotons, hyperphotons, dilatons, and moduli among others. For such particles the interaction constant α could be much larger than unity. The same holds for theories based on extra-dimensional physics with low-energy compactification scale where, for instance, for models with three extra dimensions the predicted characteristic size of extra dimensions is of about 5 nm [12,13].

To conclude this section we briefly discuss possible reasons for the observed deviations between experiment and theory at the shortest separations shown in Fig. 4a,b. These deviations are well inside the 95% confidence interval determined for $P^{\text{th}} - \bar{P}$ and thus they are not statistically meaningful. Nevertheless if we bear in mind that the deviations under consideration are several times larger than the total experimental error, there may be some underlying physics leading to the small discrepancies between experiment and theory. The most natural assumption is that there is some undiscovered nonlinearity of the oscillator which results in an additional systematic error at short separations. However, as discussed in Sec. 2, special tests of the oscillator linearity have been performed which did not reveal a nonlinear behavior for the amplitudes of sphere oscillations employed in this experiment. Another possible effect may be connected with some fine properties of interacting surfaces determined, e.g., by correlation effects in surface roughness or by patch potentials. However, as was analyzed in detail in [37], these effects are negligibly small. Thus, even assuming enormously large patches due

to monocrystals with grain sizes ranging from ~ 300 nm (i.e., larger than the film thickness) and to 25 nm, the correction to the pressure due to patches at $z = 160$ nm is only 0.42 mPa (to be compared with the deviation between experiment and theory of almost 10 mPa, as in Fig. 4a).

We next consider the possibility that the deviation may be caused by the Yukawa interaction (23) with some appropriate values of α and λ . A simple calculation shows that the deviations between experiment and theory at short separations would practically disappear if we allowed a Yukawa interaction with $\alpha = 5.0 \times 10^{21}$ and $\lambda = 10.4$ nm. This interaction would correspond to a point in Fig. 6 with $\log \lambda = -7.98$ situated slightly below line 1. However, such a point would lie above the point $\alpha = 1.0 \times 10^{20}$ with the same λ on line 2, which implies that the assumed Yukawa interaction is excluded by the AFM experiment [30]. Bearing in mind that in the above we have reanalyzed the results of [30] at a 95% confidence level using modern methods of comparison between experiment and theory, this is strong evidence against the existence of a single Yukawa interaction with $\alpha = 5.0 \times 10^{21}$ and $\lambda = 10.4$ nm. However, this analysis does not necessarily exclude the possible existence of more than one Yukawa, or other interactions having a different spatial dependence. A more decisive conclusion about the presence of hypothetical interactions can be obtained through a repetition of the experiment described in Sec. 2 using a Si plate but with no covering metallic layer. Noting that the density of Au is in 8.3 times larger than the density of Si, and that the Casimir pressure between Au and Si is approximately 1.5 times smaller than between Au and Au, the deviation caused by the Yukawa interaction should practically disappear if the Au coated plate is replaced with a Si plate.

5 Conclusions and discussion

In this paper we have presented additional details on the recent experimental determination of the Casimir pressure between two parallel plates using a micromachined oscillator. This experiment incorporates several improvements over all previous measurements. In particular, the measurements over a wide separation range were repeated many times at practically the same points for each repetition. This permits us to substantially reduce the random error, and to make it much smaller than the systematic error for the first time in Casimir force measurements. Also the plasma frequency of the Au films was determined using the measured temperature dependence of their resistivity.

The resulting experimental data were compared with a new theoretical approach to the thermal Casimir force using the Lifshitz theory incorporating a generalized plasma-like dielectric permittivity which takes into account the interband transitions. For this purpose a new oscillator fit of the tabulated optical data for the imaginary part of the dielectric permittivity of Au was performed which is more exact than a previously used fit based on DESY data. The new theoretical approach was also compared with the previously known approach using the Leontovich surface

impedance, and with the alternative approach using the Drude model. The Drude model approach was excluded experimentally at a 99.9% confidence level over a wide separation range.

One of the main aims of this paper is the application of the Casimir effect to obtain stronger constraints on hypothetical long-range interactions and light elementary particles. We have reanalyzed the previously known constraints from the measurement of the Casimir force between an Au-coated sphere and a plate using modern methods of comparison of experiment and theory at high confidence. We have also used the resulting level of agreement between the measurements of the Casimir pressure and the new theory to strengthen constraints on the hypothetical Yukawa-type interaction. The new constraints obtained above are the strongest within the interaction range from 20 to 86 nm, with the largest improvement by a factor 4.4. These results are relevant for the verification of different theoretical predictions made on the basis of unified field theories beyond the standard model, and of extra-dimensional physics. We have also discussed some possible reasons for small deviations between experiment and theory at the shortest separations considered. It was shown that although these systematic deviations are not statistically significant, the fact that we have no explanation for them at present suggests that further experimental and theoretical work is required to elucidate their nature.

Acknowledgements. R.S.D. acknowledges NSF support through Grant No. CCF-0508239. E.F. was supported in part by DOE under Grant No. DE-AC02-76ER071428. G.L.K. and V.M.M. are grateful to Purdue University for kind hospitality and financial support. They were also partially supported by DFG grant 436RUS 113/789/0-3.

References

1. E. Fischbach, C. L. Talmadge, *The Search for Non-Newtonian Gravity* (Springer-Verlag, New York, 1999).
2. E. G. Adelberger, B. R. Heckel, A. E. Nelson, *Ann. Rev. Nucl. Part. Sci.* **53**, 77 (2003).
3. Y. Fujii, *Int. J. Mod. Phys. A* **6**, 3505 (1991).
4. E. G. Adelberger, B. R. Heckel, C. W. Stubbs, W. F. Rogers, *Ann. Rev. Nucl. Part. Sci.* **41**, 269 (1991).
5. S. Dimopoulos, G. F. Giudice, *Phys. Lett. B* **379**, 105 (1996).
6. J. Sucher, G. Feinberg, in *Long-Range Casimir Forces*, eds. F. S. Levin and D. A. Micha (Plenum, New York, 1993).
7. S. D. Drell, K. Huang, *Phys. Rev.* **91**, 1527 (1953).
8. F. Ferrer, J. A. Grifols, *Phys. Rev. D* **58**, 096006 (1998).
9. G. Feinberg, J. Sucher, *Phys. Rev.* **166**, 1638 (1968).
10. E. Fischbach, *Ann. Phys. (N.Y.)* **247**, 213 (1996).
11. S. D. H. Hsu, P. Sikivie, *Phys. Rev. D* **49**, 4951 (1994).
12. I. Antoniadis, N. Arkani-Hamed, S. Dimopoulos, G. Dvali, *Phys. Lett. B* **436**, 257 (1998).
13. N. Arkani-Hamed, S. Dimopoulos, G. Dvali, *Phys. Lett. B* **429**, 263 (1998); *Phys. Rev. D* **59**, 086004 (1999).
14. A. Kehagias, K. Sfetsos, *Phys. Lett. B* **472**, 39 (2000).
15. E. G. Floratos, G. K. Leontaris, *Phys. Lett. B* **465**, 95 (1999).
16. C. Kokorelis, *Nucl. Phys. B* **677**, 115 (2004).
17. L. Randall, R. Sundrum, *Phys. Rev. Lett.* **83**, 3370 (1999); **83**, 4690 (1999).
18. A. A. Saharian, *Phys. Rev. D* **74**, 124009 (2006).
19. I. Antoniadis, *Int. J. Mod. Phys. A* **21**, 1657 (2006).
20. M. Kardar and R. Golestanian, *Rev. Mod. Phys.* **71**, 1233 (1999).
21. G. L. Smith, C. D. Hoyle, J. H. Gundlach, E. G. Adelberger, B. R. Heckel, H. E. Swanson, *Phys. Rev. D* **61**, 022001 (1999).
22. C. D. Hoyle, U. Schmidt, B. R. Heckel, E. G. Adelberger, J. H. Gundlach, D. J. Kapner, H. E. Swanson, *Phys. Rev. Lett.* **86**, 1418 (2001).
23. J. C. Long, H. W. Chan, A. B. Churnside, E. A. Gulbis, M. C. M. Varney, J. C. Price, *Nature* **421**, 922 (2003).
24. J. Chiaverini, S. J. Smullin, A. A. Geraci, D. M. Weld, A. Kapitulnik, *Phys. Rev. Lett.* **90**, 151101 (2003).
25. S. J. Smullin, A. A. Geraci, D. M. Weld, J. Chiaverini, S. Holmes, A. Kapitulnik, *Phys. Rev. D* **72**, 122001 (2005).
26. D. J. Kapner, T. S. Cook, E. G. Adelberger, J. H. Gundlach, B. R. Heckel, C. D. Hoyle, H. E. Swanson, *Phys. Rev. Lett.* **98**, 021101 (2007).
27. S. K. Lamoreaux, *Phys. Rev. Lett.* **78**, 5 (1997); **81**, 5475(E) (1998).
28. U. Mohideen, A. Roy, *Phys. Rev. Lett.* **81**, 4549 (1998); G. L. Klimchitskaya, A. Roy, U. Mohideen, V. M. Mostepanenko, *Phys. Rev. A* **60**, 3487 (1999).
29. A. Roy, C.-Y. Lin, U. Mohideen, *Phys. Rev. D* **60**, 111101(R) (1999).
30. B. W. Harris, F. Chen, U. Mohideen, *Phys. Rev. A* **62**, 052109 (2000); F. Chen, G. L. Klimchitskaya, U. Mohideen, V. M. Mostepanenko, *Phys. Rev. A* **69**, 022117 (2004).
31. T. Ederth, *Phys. Rev. A* **62**, 062104 (2000).
32. M. Bordag, B. Geyer, G. L. Klimchitskaya, V. M. Mostepanenko, *Phys. Rev. D* **58**, 075003 (1998); **60**, 055004 (1999); **62**, 011701(R) (2000).
33. J. C. Long, H. W. Chan, J. C. Price, *Nucl. Phys. B* **539**, 23 (1999).
34. V. M. Mostepanenko, M. Novello, *Phys. Rev. D* **63**, 115003 (2001).
35. E. Fischbach, D. E. Krause, V. M. Mostepanenko, M. Novello, *Phys. Rev. D* **64**, 075010 (2001).
36. R. S. Decca, E. Fischbach, G. L. Klimchitskaya, D. E. Krause, D. López, V. M. Mostepanenko, *Phys. Rev. D* **68**, 116003 (2003).
37. R. S. Decca, D. López, E. Fischbach, G. L. Klimchitskaya, D. E. Krause, V. M. Mostepanenko, *Ann. Phys. (N.Y.)* **318**, 37 (2005).
38. H. B. Chan, V. A. Aksyuk, R. N. Kleiman, D. J. Bishop, F. Capasso, *Science* **291**, 1941 (2001); *Phys. Rev. Lett.* **87**, 211801 (2001).
39. R. S. Decca, D. López, E. Fischbach, G. L. Klimchitskaya, D. E. Krause, V. M. Mostepanenko, *Phys. Rev. D* **75**, 077101 (2007).
40. G. L. Klimchitskaya, U. Mohideen, V. M. Mostepanenko, *J. Phys. A: Math. Theor.* **40**, 339(F) (2007).
41. *Handbook of Optical Constants of Solids*, ed. E. D. Palik (Academic, New York, 1985).
42. V. A. Parsegian, G. H. Weiss, *J. Colloid Interface Sci.* **81**, 285 (1981).

43. V. A. Parsegian, *Van der Waals Forces: A Handbook for Biologists, Chemists, Engineers, and Physicists* (Cambridge University Press, Cambridge, 2005).
44. M. Boström, B. E. Sernelius, Phys. Rev. Lett. **84**, 4757 (2000).
45. J. Blocki, J. Randrup, W. J. Swiatecki, C. F. Tsang, Ann. Phys. (N.Y.) **105**, 427 (1977).
46. B. V. Derjaguin, I. I. Abrikosova, E. M. Lifshitz, Q. Rev. Chem. Soc. **10**, 295 (1956).
47. M. Bordag, U. Mohideen, V. M. Mostepanenko, Phys. Rep. **353**, 1 (2001).
48. S. G. Rabinovich, *Measurement Errors and Uncertainties. Theory and Practice* (Springer-Verlag, New York, 2000).
49. G. Bressi, G. Carugno, R. Onofrio, G. Ruoso, Phys. Rev. Lett. **88**, 041804 (2002).
50. C. Yang, A. Wax, R. R. Dasari, M. S. Feld, Opt. Lett. **27**, 77 (2002).
51. S. Brandt, *Statistical and Computational Methods in Data Analysis* (North-Holland, Amsterdam, 1976).
52. T. Emig, R. L. Jaffe, M. Kardar, A. Scardicchio, Phys. Rev. Lett. **96**, 080403 (2006).
53. M. Bordag, Phys. Rev. D **73**, 125018 (2006).
54. A. Bulgac, P. Magierski, A. Wirzba, Phys. Rev. D **73**, 025007 (2006).
55. H. Gies, K. Klingmüller, Phys. Rev. Lett. **96**, 220401 (2006); Phys. Rev. D **74**, 045002 (2006).
56. D. E. Krause, R. S. Decca, D. López, E. Fischbach, Phys. Rev. Lett. **98**, 050403 (2007).
57. N. W. Ashcroft, N. D. Mermin, *Solid State Physics* (Saunders Colledge, Philadelphia, 1976).
58. *American Institute of Physics Handbook* (McGraw-Hill, New York, 1972).
59. A. Lambrecht, S. Reynaud, Eur. Phys. J. D **8**, 309 (2000).
60. E. M. Lifshitz, L. P. Pitaevskii, *Statistical Physics* (Pergamon Press, Oxford, 1980), Pt. II.
61. V. B. Bezerra, G. L. Klimchitskaya, V. M. Mostepanenko, C. Romero, Phys. Rev. A **69**, 022119 (2004).
62. C. Genet, A. Lambrecht, S. Reynaud, Phys. Rev. A **62**, 012110 (2000).
63. M. Bordag, B. Geyer, G. L. Klimchitskaya, V. M. Mostepanenko, Phys. Rev. Lett. **85**, 503 (2000); **87**, 259102 (2001).
64. V. B. Bezerra, G. L. Klimchitskaya, C. Romero, Phys. Rev. A **65**, 012111 (2002).
65. B. Geyer, G. L. Klimchitskaya, V. M. Mostepanenko, Phys. Rev. A **67**, 062102 (2003).
66. V. B. Bezerra, R. S. Decca, E. Fischbach, B. Geyer, G. L. Klimchitskaya, D. E. Krause, D. López, V. M. Mostepanenko, C. Romero, Phys. Rev. E **73**, 028101 (2006).
67. J. S. Høyve, I. Brevik, J. B. Aarseth, K. A. Milton, J. Phys. A: Math. Gen. **39**, 6031 (2006).
68. L. D. Landau, E. M. Lifshitz, L. P. Pitaevskii, *Electrodynamics of Continuous Media* (Pergamon Press, Oxford, 1984).
69. T. Emig, A. Hanke, R. Golestanian, M. Kardar, Phys. Rev. Lett. **87**, 260402 (2001).
70. C. Genet, A. Lambrecht, P. Maia Neto, S. Reynaud, Europhys. Lett. **62**, 484 (2003).
71. I. Pirozhenko, A. Lambrecht, V. B. Svetovoy, New J. Phys. **8**, 238 (2006).
72. D. Iannuzzi, I. Gelfand, M. Lisanti, F. Capasso, in: *Quantum Field Theory under the Influence of External Conditions*, ed. K. A. Milton (Rinton Press, Princeton, 2004).
73. S. K. Lamoreaux, W. T. Buttler, Phys. Rev. E **71**, 036109 (2005).
74. M. Brown-Hayes, D. A. R. Dalvit, F. D. Mazzitelli, W. J. Kim, R. Onofrio, Phys. Rev. A **72**, 052102 (2005).
75. P. Antonini, G. Bressi, G. Carugno, G. Galeazzi, G. Messineo, G. Ruoso, New J. Phys. **8**, 239 (2006).
76. G. L. Klimchitskaya, F. Chen, R. S. Decca, E. Fischbach, D. E. Krause, D. López, U. Mohideen, V. M. Mostepanenko, J. Phys. A: Math. Gen. **39**, 6485 (2006).
77. F. Chen, U. Mohideen, G. L. Klimchitskaya, V. M. Mostepanenko, Phys. Rev. A **74**, 022103 (2006).
78. R. S. Decca, D. López, H. B. Chan, E. Fischbach, D. E. Krause, C. R. Jamell, Phys. Rev. Lett. **94**, 240401 (2005).